THE JOURNAL OF PHYSICAL CHEMISTRY B

Article

Cite This: J. Phys. Chem. B 2018, 122, 1387−1393

pubs.acs.org/JPCB

Allocating and Splitting Free Energy to Maximize Molecular Machine Flux

Aidan I. Brown* and David A. Sivak*

Department of Physics, Simon Fraser University, Burnaby, British Columbia V5A1S6, Canada

Supporting Information

ABSTRACT: Biomolecular machines transduce between different forms of energy. These machines make directed progress and increase their speed by consuming free energy, typically in the form of nonequilibrium chemical concentrations. Machine dynamics are often modeled by transitions between a set of discrete metastable conformational states. In general, the free-energy change associated with each transition can increase the forward rate constant, decrease the reverse rate constant, or both. In contrast to previous optimizations, we find that in general flux is maximized neither by devoting all free-energy changes to increasing forward rate constants nor by solely decreasing reverse rate constants. Instead, the optimal free-energy splitting depends on the detailed dynamics. Extending our analysis to machines with vulnerable states (from which they can break down), in the strong driving corresponding to in vivo cellular conditions, processivity is maximized by reducing the occupation of the vulnerable state.

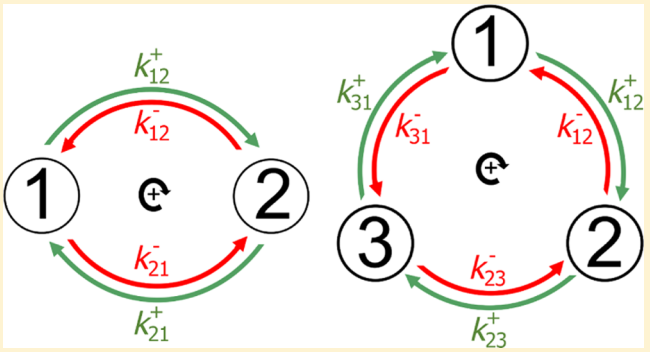

INTRODUCTION

Molecular machines such as kinesin,[1] helicase,[2] and ubiquitin ligase[3] perform diverse tasks inside cells. These machines typically convert nonequilibrium chemical concentrations, maintained by other machinery in the cell,[4,5] into directed motion or work.[6,7] These microscopic machines operate stochastically,[8] with their fluctuating progress now experimentally observable with improving resolution (see, e.g., Isojima et al.[9]).

Quantitative models of molecular machines are pervasive, for example to investigate forces,[10,11] efficiency,[12,13] and performance of different driving mechanisms.[14,15] Each model usually treats molecular machine dynamics as a set of transitions between discrete metastable states,[16] as diffusion on a continuous energy landscape,[17] or a combination of the two.[18]

In this article, we study how the flux of cyclic machines, a posited driver of evolutionary fitness,[19] is affected by the details of free-energy changes over a set of discrete states.

Earlier models considered how the influence of a load is quantitatively split between forward and reverse transitions.[11,13,14,16] In this work, we find that by extending the splitting to all free-energy components, and not just loads, there is no single splitting scheme that always maximizes the flux. Additionally, optimizing the allocation of a single free-energy component compensates for any suboptimal fixed allocations of other free-energy components.

We also examine how to maximize progress for transiently processive cyclic machines with vulnerable states, from which the machine can break down or "escape" (e.g., kinesin can dissociate from a microtubule[20]). For strong driving, free energy is simply allocated to reduce the occupation of the state vulnerable to escape. However, under specific conditions, the optimal allocation is reversed, counterintuitively increasing processivity by increasing occupation of the vulnerable state.

MODEL

Discrete States. We consider cycles with two or three states (Figure 1), often used for models of molecular motors or other driven systems inside living cells.[21,22] For our model

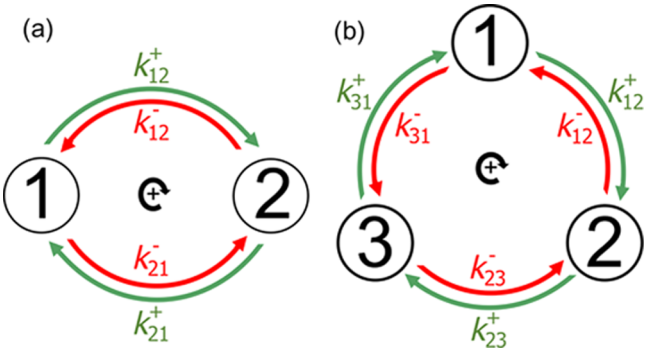

Figure 1. Discrete-state cycles with (a) two and (b) three states. Transitions occur in both the forward (green arrows) and reverse (red arrows) directions for each pathway between two states, described by the respective rate constants k_{ij}^{+} and k_{ij}^{-}.

Received: October 26, 2017
Revised: December 20, 2017
Published: January 1, 2018

DOI: 10.1021/acs.jpcb.7b10621
J. Phys. Chem. B 2018, 122, 1387−1393

cycles, each forward rate constant k_{ij}^{+} describes transitions from state i to state j, with a corresponding reverse rate constant k_{ij}^{-} for transitions from state j to state i. To preserve microscopic reversibility,[11,15] any transition with a nonzero forward rate cannot be irreversible and must also have a nonzero reverse rate.

Forward transitions from state i to state j occur at rate $k_{ij}^{+}P_i$, for probability P_i in state i. Reverse transitions from state j to state i occur at reverse rate $k_{ij}^{-}P_j$. (The two-state cycle has two pathways, 12 and 21, each with a forward and reverse direction, and each representing distinguishable physical transition mechanisms.)

To preferentially drive such cycles in a particular direction, cells use nonequilibrium concentrations of reacting chemical species, such as adenosine triphosphate (ATP), adenosine diphosphate (ADP), and inorganic phosphate (P_i).[23] ATP hydrolysis into ADP and P_i yields a free energy, ΔG, that depends on the respective concentrations[23]

$$\Delta G = \Delta G_0 + k_B T \ln \frac{[\mathrm{ADP}][\mathrm{P_i}]}{[\mathrm{ATP}]} \tag{1}$$

Here, $\Delta G_0 \equiv -k_B T \ln([\mathrm{ADP}]_{eq}[\mathrm{P_i}]_{eq}/[\mathrm{ATP}]_{eq})$, k_B is Boltzmann's constant, and T is the temperature of the thermal bath exchanging heat with the system. ATP hydrolysis provides free energy $|\Delta G| \sim 20 k_B T$ under typical physiological conditions.[23] From here on, we set $k_B T = 1$, thus measuring all free energies in units of the thermal energy scale, $k_B T$.

The free-energy allocation, ω_{ij}, of a given transition path fixes the ratio between the forward and reverse rate constants[14,24,25]

$$\omega_{ij} = \ln \frac{k_{ij}^{+}}{k_{ij}^{-}} \tag{2}$$

Without ω_{ij} to provide a bias, the full forward and reverse rate constants, $k_{ij}^{+/-}$, are each equal to the "bare" rate constants, k_{ij}^{0}. $\omega_{ij} = -\Delta G_{ij}$, where ΔG_{ij} is the free-energy change of the machine and its surroundings over the transition. ΔG over a given cycle must be negative to drive net progress in the forward direction (on average).

Biasing Rates with Free Energy. ω_{ij} can be composed of several different free-energy components, including but not limited to conformational changes, binding/unbinding, or a change in potential.

The free-energy change ΔG_{ij}^{mach} of the molecular machine over a transition includes free-energy differences between distinct machine conformations, as well as changes in the free energy of any molecules bound to the machine (e.g., hydrolysis of ATP to ADP and P_i), as the free-energy changes of the machine and bound species cannot be separated.[26,27]

$\Delta G_{ij}^{bind} = -\mu$ is the free-energy change of the solution when a molecule binds the machine, leaving the solution, with μ the chemical potential of the molecule given the concentration in solution. ΔG_{ij}^{bind} includes molecules typically considered "fuel", such as ATP, and those typically considered cargo. For a molecule that unbinds from the machine and joins the solution, $\Delta G_{ij}^{unbind} = \mu$.

ΔG_{ij}^{pot} represents the free-energy change of the machine or any object attached to the machine, due to an external potential or gradient, for example, due to a bead attached to kinesin that is also in an optical trap.

Similar frameworks have typically been applied to the analysis of molecular motors that perform mechanical work; however, we cast our theory at a level of generality that in principle applies equally well to catalytic enzymes,[28] signal transducers,[29] and other stochastic machines.

We confine our attention in this article to "reversible" free-energy components, whereby any free energy expended in a forward reaction is recovered by the reverse reaction. Thus, we exclude from consideration any omnidirectional free-energy dissipation,[30,31] such as that due to friction when pulling a load through a viscous medium.

Except for ΔG_{ij}^{mach}, we expect that the free-energy components are relatively fixed (i.e., unable to be changed by a modification to the machine). $\sum \Delta G_{ij}^{mach} = 0$, as the machine returns to the same state after completing each cycle; abiding by this constraint, variation of ΔG_{ij}^{mach} (nominally through machine mutations) can be used to optimize machine operation.

We model each free-energy component $\omega_{ij}^{k} = -\Delta G_{ij}^{k}$ with a different splitting factor[13,14] $\delta_{ij}^{k} \in [0,1]$, which describes how the effect of ω_{ij}^{k} is divided between forward and reverse rate constants

$$k_{ij}^{+} \propto e^{\sum_k \delta_{ij}^{k} \omega_{ij}^{k}} \text{ and } k_{ij}^{-} \propto e^{-\sum_k (1-\delta_{ij}^{k}) \omega_{ij}^{k}} \tag{3}$$

Our restriction to $\delta \in [0,1]$ is typical for chemical kinetics, but excludes catch bonds.[32]

Earlier studies[11,13,14,16] considered a molecular motor pulling against a constant opposing force, F, with each cycle of the motor stepping forward a distance, d. The transition completing the step transduces free energy $w = Fd$ to the motor's position in the potential. In our framework, this corresponds to $\omega_{ij}^{pot} = -w$. For steps against this constant force, some refer to $\delta_{ij}^{pot} = 0$ as a power stroke and $\delta_{ij}^{pot} = 1$ as a Brownian ratchet.[14]

In this article, we primarily consider the case where splitting factors, δ_{ij}^{k}, have the same value, δ, for all free-energy components. This simple framework assumes that the transition state is similarly arrayed between the reactant and the product along different coordinate axes. We label $\delta = 1$ as forward labile (FL) and $\delta = 0$ as reverse labile (RL). The choice between FL and RL affects machine performance characteristics,[14,33] and next we determine how to vary splitting factors to maximize flux.

RESULTS

Optimal Splitting Factors. Setting all splitting factors, δ_{ij}^{k}, to the same value, δ, allows the combination of all $\delta_{ij}^{k}\omega_{ij}^{k}$ terms in eq 3 into single terms, $\delta\omega_{ij}$ and $(1-\delta)\omega_{ij}$, giving rate constants

$$k_{ij}^{+} = k_{ij}^{0}\, e^{\delta \omega_{ij}} \tag{4a}$$

$$k_{ij}^{-} = k_{ij}^{0}\, e^{-(1-\delta)\omega_{ij}} \tag{4b}$$

We consider a two-state cycle, with steady-state flux (hereafter simply flux)[34]

$$J = \frac{k_{12}^{+}k_{21}^{+} - k_{12}^{-}k_{21}^{-}}{k_{12}^{+} + k_{12}^{-} + k_{21}^{+} + k_{21}^{-}} \tag{5}$$

Inserting eqs 4a and 4b into eq 5 and differentiating with respect to δ gives

DOI: 10.1021/acs.jpcb.7b10621
J. Phys. Chem. B 2018, 122, 1387−1393

$$\frac{\partial J}{\partial \delta} = \frac{(1 - e^{-\omega_{tot}})[k_{12}^0 \omega_{21} e^{-\delta\omega_{21}}(1 + e^{-\omega_{12}}) + k_{21}^0 \omega_{12} e^{-\delta\omega_{12}}(1 + e^{-\omega_{21}})]}{[(k_{21}^0)^{-1} e^{-\delta\omega_{21}}(1 + e^{-\omega_{12}}) + (k_{12}^0)^{-1} e^{-\delta\omega_{12}}(1 + e^{-\omega_{21}})]^2} \quad (6)$$

The cycle proceeds forward when $\omega_{tot} = \omega_{12} + \omega_{21} > 0$. $\partial J/\partial\delta > 0$ for all δ when both $\omega_{12} > 0$ and $\omega_{21} > 0$; for these conditions, $\delta = 1$ (FL) maximizes the flux. For $\delta = 0$ (RL) to maximize the flux requires

$$k_{12}^0 \omega_{21}(1 + e^{-\omega_{12}})\, e^{-\delta\omega_{21}} + k_{21}^0 \omega_{12}(1 + e^{-\omega_{21}})\, e^{-\delta\omega_{12}} < 0 \quad (7)$$

a more complicated condition to fulfill, as $\omega_{12} < 0$ and $\omega_{21} < 0$ cannot be simultaneously fulfilled with $\omega_{tot} > 0$. Flux can also be maximized for intermediate δ, with $\partial J/\partial\delta$ changing sign (maximizing flux) when

$$\delta = \frac{1}{\omega_{21} - \omega_{12}} \ln\left[-\frac{k_{12}^0 \omega_{21}(1 + e^{-\omega_{12}})}{k_{21}^0 \omega_{12}(1 + e^{-\omega_{21}})}\right] \quad (8)$$

The flux-maximizing value of splitting factor δ thus depends on free-energy allocation ω_{ij} and bare rate constants k_{ij}^0.

Although here we set $\delta_{ij}^k = \delta$, in Supporting Information (SI: Varying splitting factors), we consider splitting factors δ_{ij}^k that vary across different free-energy components and different transitions. Notably, for splitting factors specific to each free-energy component k and transition ij, if $\omega_{ij}^k < 0$, then $\delta_{ij}^k = 0$ maximizes the flux, and if $\omega_{ij}^k > 0$, then $\delta_{ij}^k = 1$ maximizes the flux.

For a molecular motor pulling against a constant force, a forward step has free-energy component $\omega_{ij}^{pot} = -w < 0$. For independent variation of δ_{ij}^k, flux is maximized for $\delta_{ij}^{pot} = 0$. In this scenario, the optimal splitting factor agrees with Wagoner and Dill's finding that $\delta = 0$ maximizes the power.[14] Our results are generally distinct and do not find a universal optimal δ value because we generalize to cycles with multiple states and splitting factors that apply to all free-energy components, not just the free-energy component associated with pulling against a constant force.

Figure 2 shows the variation in flux as the splitting factor, δ, is varied from the flux-maximizing value in the range $\delta \in [0,1]$. The flux can be maximized at an extreme splitting factor value, $\delta = 1$ (left panels) or 0 (not shown, but possible), or between the extreme values, $\delta \in (0,1)$ (right panels). The flux can decrease by more than an order of magnitude away from the optimal δ value and decreases faster for larger ω_{tot}.

Optimal Free-Energy Allocation. Considering eqs 4a and 4b, we vary the free energy, ω_{ij}, allocated to each transition to adjust the rate constants and maximize the flux.

For the total free-energy budget per cycle $\omega_{tot} = \omega_{12} + \omega_{21}$, the flux-maximizing free-energy allocation, ω_{12}^*, satisfies (see SI: Varying free energy)

$$k_{12}^0\, e^{\delta\omega_{12}^*}[\delta - (1 - \delta)\, e^{-\omega_{12}^*}] = k_{21}^0\, e^{\delta(\omega_{tot} - \omega_{12}^*)}[\delta - (1 - \delta)\, e^{-(\omega_{tot} - \omega_{12}^*)}] \quad (9)$$

This cannot generally be solved for ω_{12}^*.

For equal splitting factors $\delta_{ij}^k = \delta$, rate constants are determined by the sum of all free-energy components $\sum_k \omega_{ij}^k$, such that if all but one free-energy component is fixed, the remaining free-energy component can be varied to achieve any desired sum. This makes maximal flux attainable by only adjusting the free-energy allocation of the molecular machine, ΔG_{ij}^{mach}.

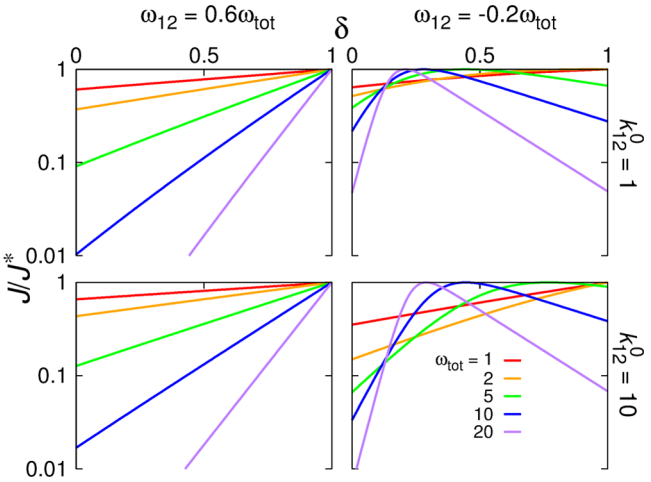

Figure 2. Two-state flux sensitivity to splitting factor. Flux ratio J/J^* as a function of the splitting factor δ, for a two-state cycle with bare rate $k_{21}^0 = 1$. k_{12}^0, ω_{tot}, and ω_{12} vary as indicated. J is given by substituting the rate constants of eqs 4a and 4b into eq 5. J^* is determined in the range $\delta \in [0,1]$. Optimal flux J^* is specific to each curve on each subplot.

For $\delta = 0$ and 1, the rate constants reduce to those of our previous work,[33] from which the flux-maximizing free-energy allocation, ω_{ij}^*, can be determined. For $\delta = 1$ (FL)

$$\omega_{12}^* = \frac{1}{2}\omega_{tot} + \frac{1}{2}\ln\frac{k_{21}^0}{k_{12}^0} \quad (10)$$

For $\delta = 0$ (RL)

$$\omega_{12}^* = \frac{1}{2}\omega_{tot} - \frac{1}{2}\ln\frac{k_{21}^0}{k_{12}^0} \quad (11)$$

ω_{ij} may be decomposed into multiple free-energy components; for conceptual clarity, we limit our discussion to two, $\omega_{ij} = \omega_{ij}^{I} + \omega_{ij}^{II}$, but our results trivially generalize. With $\omega_{ij}^* = \omega_{ij}^{I*} + \omega_{ij}^{II*}$, $\sum\omega_{ij}^{I} = \omega_{tot}^{I}$, and $\sum\omega_{ij}^{II} = \omega_{tot}^{II}$, then for $\delta = 1$, eq 10 becomes

$$\omega_{12}^{I*} + \omega_{12}^{II*} = \frac{1}{2}(\omega_{tot}^{I} + \omega_{tot}^{II}) + \frac{1}{2}\ln\frac{k_{21}^0}{k_{12}^0} \quad (12)$$

If one component is fixed (without loss of generality ω_{ij}^{II}), then ω_{ij}^{I} can vary to preserve the flux-maximizing allocation $\omega_{ij}^* = \omega_{ij}^{I*} + \omega_{ij}^{II*}$. Effectively, the variable component of ω_{ij} can compensate for the fixed component to maximize the flux.

In earlier work,[33] we showed that for a range of several k_BT around the optimal allocation, the flux can decrease by more than an order of magnitude. The free-energy allocation can thus meaningfully alter the cycle output.

In this section, we considered equal splitting factors for all free-energy components and transitions: $\delta_{ij}^k = \delta$. In SI: Varying free energy, we consider the more general case where the splitting factor varies over free-energy components and transitions, similarly finding that variable free-energy components compensate for fixed components.

Robustness to Variable Load. The in vivo operating environment of molecular machines is diverse, with variable cargo, molecular concentrations, and other factors causing some free-energy components to vary over the life cycle of a machine. We consider a scenario with two free-energy components over a cycle, ω_{tot}^{I} and ω_{tot}^{II}. ω_{tot}^{I} has some fixed

DOI: 10.1021/acs.jpcb.7b10621
J. Phys. Chem. B 2018, 122, 1387−1393

value, but ω^{II}_{tot} is a load that can be applied or removed, with $\omega^{II}_{tot} = 0$ (no load) or $\omega^{II}_{tot} = -w_{tot} < 0$ (load). The allocation of ω^{II}_{tot} to the various ω^{II}_{ij} is fixed. If the allocation of ω^{I}_{ij} is optimized without (with) an applied load, but then the load is applied (removed), the flux will generally be lower than if ω^{I}_{ij} is optimized under the correct conditions. Figure 3 shows the flux

Figure 3. Robustness to variable load. Flux J vs load w_{tot} for a two-state forward labile ($\delta^k_{ij} = \delta = 1$) cycle. The load is entirely on the first transition, $\omega^{II}_{12} = -w_{tot}$, and $\omega^{II}_{21} = 0$. Bare rate constants $k^0_{12} = 5$, $k^0_{21} = 1$, and load-free free-energy budget $\omega^{I}_{tot} = 20$. Solid curves are for $\omega^{I*,no\ load}_{ij}$ optimized for no load, whereas dashed curves are for $\omega^{I*,load}_{ij}$ optimized with load w_{tot}. Black curves show flux without load ($w_{tot} = 0$), whereas red curves show flux with load w_{tot}, as indicated by the horizontal axis.

as a function of load for $\omega^{I}_{tot} = 20k_BT$ (that of ATP under physiological conditions) for the four possible scenarios, optimized with ($\omega^{I*,load}_{ij}$) or without ($\omega^{I*,no\ load}_{ij}$) load and subsequently applying or not applying a load.

The fluxes for the four scenarios have a fixed order, independent of model parameters. Without load, cycle flux is higher under the correctly optimized allocation, $\omega^{I*,no\ load}_{ij}$, than under the incorrectly optimized one for load, $\omega^{I*,load}_{ij}$; under $\omega^{I*,load}_{ij}$, the flux is higher without load than with it because adding a resistive load always reduces the flux; with load, flux under the correctly optimized $\omega^{I*,load}_{ij}$ is higher than under the incorrectly optimized $\omega^{I*,no\ load}_{ij}$. Owing to this fixed ordering, the flux changes less when the load is applied or removed if the free-energy component allocation is optimized with a load ($\omega^{I*,load}_{ij}$), compared to if the allocation is optimized for no load ($\omega^{I*,no\ load}_{ij}$).

Processivity. Many cycles are transiently processive, eventually "escaping" from their processive mode of operation, precluding further progress. For example, a transport motor can detach from its cytoskeletal track and diffuse away, effectively ending its forward transport.[20,35]

We model escape from a single "vulnerable" state (without loss of generality, state 2), consistent with experiments suggesting that kinesin primarily detaches from a subset of states.[20,36−39] The vulnerable state has an escape rate constant, k_{esc}. The states that are not vulnerable have the same dynamics as mentioned earlier. For the two-state cycle, escape produces modified state 2 dynamics

$$\frac{dP_2}{dt} = (k^+_{12} + k^-_{21})P_1 - (k^-_{12} + k^+_{21})P_2 - k_{esc}P_2 \tag{13}$$

For $k_{esc} > 0$, probability leaves the cycle and there are no steady states for occupation probabilities P_i (except $P_1 = P_2 = 0$). Instead, we find steady states for fractional probabilities P_i/P_{tot} (see SI: Processivity), for total remaining probability $P_{tot} = \sum_i P_i$. This determines the dynamics of P_{tot} and thus the average fluxes in the cycle at all times, t: $P_{tot}(t) = \exp[-k_{esc}(P_2/P_{tot})t]$.

Unlike a cycle without escape, in the steady state of P_i/P_{tot}, the fluxes for the different transitions will not generally be equal. For the two-state cycle, the changes in probabilities P_1, P_2 are determined by the flux into and out of the respective states

$$\frac{dP_1}{dt} = J_{21} - J_{12} \tag{14a}$$

$$\frac{dP_2}{dt} = J_{12} - J_{21} - J_{esc} \tag{14b}$$

Once P_i/P_{tot} reaches steady state, $dP_i/dt = P_i\, d\ln P_{tot}/dt$. Substituting this into eqs 14a and 14b and rearranging gives the pathway (or one-sided) steady-state flux

$$J_{12} = J_{21} + \frac{P_1}{P_1 + P_2}J_{esc} \tag{15}$$

Accumulated Flux. Because the flux decays with time as probability escapes, we additionally include the rate of escape in our evaluation of molecular machine progress. Instead of flux alone, we combine flux and (avoided) escape into the "accumulated flux"

$$\Phi_{acc}(t) = \int_0^t [J_{12}(t') + J_{21}(t')]\, dt' \tag{16}$$

For $t \to \infty$, Φ_{acc} can always be increased by adjusting ω_{ij} to reduce P_2/P_{tot} and thus reduce escape, so $\Phi_{acc}(\infty)$ has no maximum, and hence we maximize $\Phi_{acc}(t)$ after finite time t.

For simplicity, we consider two-state cycles with a single splitting factor $\delta^k_{ij} = \delta$. We set bare rate constants $k^0_{12} = k^0_{21} = 1$, such that all escape rate constants k_{esc} are in units of this bare rate. Figure 4 shows two-state free-energy allocations that maximize accumulated flux $\Phi_{acc}(t)$ for FL and RL schemes at various finite times t, for two distinct escape rate constants k_{esc}

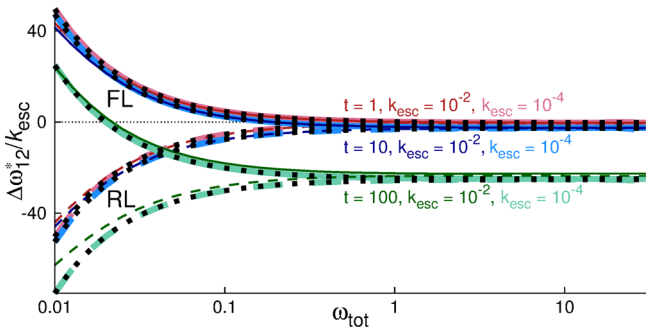

Figure 4. Allocating free energy to maximize processivity. Free energy allocation, ω_{12}, that maximizes accumulated flux, Φ_{acc} (eq 16), over varying integration times t (indicated by curve color), in an FL (solid lines) or RL (dashed) two-state cycle with $k^0_{12} = k^0_{21} = 1$ and escape rate $k_{esc} = 10^{-2}$ or 10^{-4}. Thick black dotted curves show eqs 17 and 18, which approximate $\Delta\omega^*_{12}/k_{esc}$ with low k_{esc} for FL and RL, respectively. Allocation is shown as the difference, $\Delta\omega^*_{ij} = \omega^*_{ij} - \frac{1}{2}\omega_{tot}$, from the "naive" allocation of equal free energy, $\frac{1}{2}\omega_{tot}$, to each transition. $\Delta\omega^*_{21} = -\Delta\omega^*_{12}$ is not shown. Initial condition is steady state for P_i/P_{tot}.

DOI: 10.1021/acs.jpcb.7b10621
J. Phys. Chem. B 2018, 122, 1387−1393

(see SI: Processivity for similar three-state results). These escape rate constants are consistent with modeling that suggests that the detachment time scale from the vulnerable state of myosin V is 10−1000× slower than the other time scales in the main forward pathway at zero force.[40]

A prominent feature of Figure 4 is the approximate collapse of cycles with different k_{esc} to the same $\Delta\omega_{12}^*/k_{esc}$ (where $\Delta\omega_{12}^* = \omega_{12} - \frac{1}{2}\omega_{tot}$), demonstrating that the optimal free-energy allocation $\Delta\omega_{12}^* \propto k_{esc}$ for the parameter values shown in Figure 4 (SI: Processivity shows optimal allocations for larger t, which do not collapse). For FL cycles with small k_{esc} and t

$$\frac{\Delta\omega_{12}^*}{k_{esc}} \simeq -\frac{1}{4}\left(t - \frac{1}{e^{\frac{1}{2}\omega_{tot}} - 1}\right) \tag{17}$$

and for RL

$$\frac{\Delta\omega_{12}^*}{k_{esc}} \simeq -\frac{1}{4}\left(t + \frac{1}{1 - e^{-\frac{1}{2}\omega_{tot}}}\right) \tag{18}$$

See SI: Processivity for derivations. In Figure 4, eqs 17 and 18 (thick black dotted curves) closely match the numerical $\Delta\omega_{12}^*/k_{esc}$ (solid and dashed curves) for low k_{esc} and low t.

For high free-energy budget ω_{tot}, the allocation, ω_{12}^*, in Figure 4 is intuitive: ω_{12}^* is low and (although not shown in the figure) $\omega_{21}^* = \omega_{tot} - \omega_{12}^*$ is high, reducing the probability of being in vulnerable state 2. For higher escape rates and longer times, the difference, $|\Delta\omega_{ij}^*|$, between optimal and naive allocations increases, diverging as time $t \to \infty$.

In Figure 4, $\Delta\omega_{12}^*$ for FL changes sign from negative to positive as ω_{tot} decreases, with the change occurring at larger ω_{tot} for shorter times. Positive $\Delta\omega_{12}^*$ increases the probability in the vulnerable state and increases the escape rate. However, maximizing Φ_{acc} is a trade-off between reducing escape and increasing ongoing flux. For longer times t and higher ω_{tot}, it is more important to reduce escape to preserve the future flux, and the intuitive result ($\Delta\omega_{12}^* < 0$) is observed. However, at small t and ω_{tot}, initial flux is relatively more important, as little escape occurs before time t is reached. The escaping flux from state 2 causes $P_1 > P_2$ for naive free-energy allocation $\omega_{12} = \omega_{21} = \frac{1}{2}\omega_{tot}$. FL only allows the forward fluxes to be increased; to maximize the flux, the forward flux for transition 12 should be increased more because $P_1 > P_2$, leading to $\Delta\omega_{12}^* > 0$. In contrast, RL only allows reverse fluxes to be decreased; to maximize the flux, the reverse flux for transition 21 should be decreased more, again because $P_1 > P_2$, consistently leading to $\Delta\omega_{12}^* < 0$.

DISCUSSION

Biomolecular machines perform a variety of tasks inside cells, driven by the free energy stored in intracellular chemical concentrations. Here, we investigated how to maximize flux in molecular machines with multiple free-energy components and how to maintain processivity.

Central to our approach is the general manner in which forward and reverse rate constants are affected by free-energy changes.[13,14,33] Free-energy components that only affect the forward or reverse rate constants represent extremes, and the division of the effect of free-energy components between the forward and reverse rate constants is more generally described by a splitting factor $\delta \in [0,1]$. We primarily consider the simplifying case where splitting factors for all distinct free-energy components are equal.

In contrast with previous results,[14] we find that no single splitting factor δ generally maximizes the flux. Instead, the optimal splitting factor depends on the detailed free-energy allocation, with flux decreasing significantly away from the optimal splitting factor (Figure 2).

Previous studies[13,14] argued that low splitting factors are optimal, suggesting low splitting factors would describe the operation of evolved biomolecular machines. We have shown that both low and high splitting factors can maximize flux and that the optimal splitting factor value depends on the allocation of free energy. Experimental fits of splitting factors find both low splitting factors[13,21,41−43] and high splitting factors.[42,44] These fits use several models for the dependence of rate constants on resisting forces.[13,21,41−45] Unlike in our model, all other models we have found assume that rate constants only explicitly contain splitting factors for force, with no splitting factors for other free-energy components (though one other model has implicit splitting of the effect of chemical potential[13]). Splitting factor analysis has largely been performed in the context of "canonical" molecular machines, such as the walking motors kinesin,[42−45] myosin,[13,21] and dynein,[46] or the rotary motor F1-ATPase.[41] Splitting factors δ are not always robust, with distinct data sets for kinesin motility[47,48] leading to substantially different inferred values of 0.3 and 0.65.[44] It would be an interesting follow-up to investigate splitting factors for all free-energy components affecting rate constants and for a broader class of molecular machines, which may lead to a broader diversity of splitting factor values. In SI: Experimental splitting factors, we describe in more detail the fitted splitting factors for various models.[13,21,41−45]

Flux can also be maximized by varying free-energy components ω_{ij}^k, with flux significantly decreasing away from the optimal, ω_{ij}^{k*}. For a scenario with two distinct free-energy components, one variable and one fixed, the flux is maximized by allocating the variable free-energy component to compensate for any departure from optimal of the fixed free-energy component allocation. There are examples of machine models fit to experimental data where transitions with a fixed load appear to receive more of the other free-energy components than those without a load (consistent with our predictions),[1,42,43] but also counterexamples that do not fit this optimal framework.[21,45]

Through mutation, biomolecular machine operation can change, and we expect evolution to select machine parameters that favor certain performance characteristics. We argue that robustness increases when tuning parameters to maximize flux with a load, rather than without a load, because for load-optimized parameters the flux is less sensitive to the presence or absence of load. This is consistent with observations of kinesin maintaining a stable velocity under a range of forces,[49] an intuitively beneficial trait.[50]

We also examined cycles that are transiently processive and escape from a single vulnerable state. For large free-energy budgets, maximizing the number of complete cycles before the cycle escapes leads to intuitive allocations: free energy is primarily allocated to decrease the probability present in the vulnerable state. However, for small free-energy budgets, to maximize the number of cycles completed, free energy is primarily allocated to increase the flux; for forward labile cycles this increases the probability present in the vulnerable state, whereas for reverse labile cycles this decreases it. Although this

DOI: 10.1021/acs.jpcb.7b10621
J. Phys. Chem. B 2018, 122, 1387−1393

forward labile allocation increases the rate of escape, the associated flux increases more than compensates, leading to an overall increase in the accumulated flux.

Kinesin mutated to have different neck linker charge shows increased processivity, which is attributed to shorter waiting times in states vulnerable to detachment from the microtubule.[36,39,51] These findings are consistent with our result that occupation of the vulnerable state should be reduced to maximize processivity for large free-energy budgets, such as the $\sim 20 k_B T$ of free energy from ATP hydrolysis[23] driving each kinesin cycle.[52]

Although we are unaware of other modeling that maximizes processivity, Hill modeled escape as a transition to the initial state where all trajectories begin, effectively acting as an additional subcycle.[53] This steady state with immediate rebinding is distinct from our steady state without rebinding. Both Hill's approach and ours allow calculation of detachment rates (distinct due to differing steady states); however, our approach additionally quantifies progress before detachment.

■ ASSOCIATED CONTENT

Supporting Information

The Supporting Information is available free of charge on the ACS Publications website at DOI: 10.1021/acs.jpcb.7b10621.

Additional calculations, model details, and detailed background on experimental fitting parameters cited from the literature (PDF)

■ AUTHOR INFORMATION

Corresponding Authors

*E-mail: aidanb@sfu.ca (A.I.B.).
*E-mail: dsivak@sfu.ca (D.A.S.).

ORCID

Aidan I. Brown: 0000-0002-6600-8289
David A. Sivak: 0000-0003-4815-4722

Notes

The authors declare no competing financial interest.

■ ACKNOWLEDGMENTS

This work was supported by a Natural Sciences and Engineering Research Council of Canada (NSERC) Discovery Grant, by funds provided by the Faculty of Science, Simon Fraser University, through the President's Research Start-up Grant, by a Tier II Canada Research Chair, and by WestGrid (www.westgrid.ca) and Compute Canada Calcul Canada (www.computecanada.ca). The authors thank Emma Lathouwers and Steven Large (SFU Physics) for useful discussions and feedback.

■ REFERENCES

(1) Clancy, B. E.; Behnke-Parks, W. M.; Andreasson, J. O. L.; Rosenfeld, S. S.; Block, S. M. A Universal Pathway for kinesin stepping. *Nat. Struct. Mol. Biol.* **2011**, *18*, 1020−1027.
(2) Caruthers, J. M.; McKay, D. B. Helicase structure and mechanism. *Curr. Opin. Struct. Biol.* **2002**, *12*, 123−133.
(3) Cardozo, T.; Pagano, M. The SCF ubiquitin ligase: Insights into a molecular machine. *Nat. Rev. Mol. Cell Biol.* **2004**, *5*, 739−751.
(4) Boyer, P. D. The ATP synthase − a splendid molecular machine. *Annu. Rev. Biochem.* **1997**, *66*, 717−749.
(5) Fernie, A. R.; Carrari, F.; Sweetlove, L. J. Respiratory metabolism: Glycolysis, the TCA cycle and mitochondrial electron transport. *Curr. Opin. Plant Biol.* **2004**, *7*, 254−261.
(6) Vale, R. D.; Milligan, R. A. The way things move: Looking under the hood of molecular motor proteins. *Science* **2000**, *288*, 88−95.
(7) Bustamante, C.; Keller, D.; Oster, G. The physics of molecular motors. *Acc. Chem. Res.* **2001**, *34*, 412−420.
(8) Astumian, R. D.; Bier, M. Fluctuation driven ratchets: Molecular motors. *Phys. Rev. Lett.* **1994**, *72*, 1766−1769.
(9) Isojima, H.; Iino, R.; Niitani, Y.; Noji, H.; Tomishige, M. Direct observation of intermediate states during the stepping motion of kinesin-1. *Nat. Chem. Biol.* **2016**, *12*, 290−297.
(10) Qian, H. A simple theory of motor protein kinetics and energetics. *Biophys. Chem.* **1997**, *67*, 263−267.
(11) Fisher, M. E.; Kolomeisky, A. B. The force exerted by a molecular motor. *Proc. Natl. Acad. Sci. U.S.A.* **1999**, *96*, 6597−6602.
(12) Qian, H. A simple theory of motor protein kinetics and energetics II. *Biophys. Chem.* **2000**, *83*, 35−43.
(13) Schmiedl, T.; Seifert, U. Efficiency of molecular motors at maximum power. *Europhys. Lett.* **2008**, *83*, 30005.
(14) Wagoner, J. A.; Dill, K. A. Molecular motors: Power strokes outperform Brownian ratchets. *J. Phys. Chem. B* **2016**, *120*, 6327−6336.
(15) Astumian, R. D. Irrelevance of the power stroke for the directionality, stopping force, and optimal efficiency of chemically driven molecular machines. *Biophys. J.* **2015**, *108*, 291−303.
(16) Thomas, N.; Imafaku, Y.; Tawada, K. Molecular motors: Thermodynamics and the random walk. *Proc. R. Soc. B* **2001**, *268*, 2113−2122.
(17) Astumian, R. D.; Mukherjee, S.; Warshel, A. The physics and physical chemistry of molecular machines. *ChemPhysChem* **2016**, *17*, 1719−1741.
(18) Xing, J.; Wang, H.; Oster, G. From continuum Fokker-Planck models to discrete kinetic models. *Biophys. J.* **2005**, *89*, 1551−1563.
(19) Nguyen, V.; Wilson, C.; Hoemberger, M.; Stiller, J. B.; Agafonov, R. V.; Kutter, S.; English, J.; Theobald, D. L.; Kern, D. Evolutionary drivers of thermoadaptation in enzyme catalysis. *Science* **2017**, *355*, 289−294.
(20) Milic, B.; Andreasson, J. O. L.; Hancock, W. O.; Block, S. M. Kinesin processivity is gated by phosphate release. *Proc. Natl. Acad. Sci. U.S.A.* **2014**, *111*, 14136−14140.
(21) Kolomeisky, A. B.; Fisher, M. E. A simple kinetic model describes the processivity of myosin-V. *Biophys. J.* **2003**, *84*, 1642−1650.
(22) Qian, H. Open-system nonequilibrium steady state: Statistical thermodynamics, fluctuations, and chemical oscillations. *J. Phys. Chem. B* **2006**, *110*, 15063−15074.
(23) Phillips, R.; Kondev, J.; Theriot, J.; Garcia, H. *Physical Biology of the Cell*, 2nd ed.; Garland Science: New York, 2012.
(24) Pietzonka, P.; Barato, A. C.; Seifert, U. Universal bound on the efficiency of molecular motors. *J. Stat. Mech.: Theory Exp.* **2016**, No. 124004.
(25) Rao, R.; Esposito, M. Nonequilibrium thermodynamics of chemical reaction networks: Wisdom from stochastic thermodynamics. *Phys. Rev. X* **2016**, *6*, No. 041064.
(26) Hill, T. L.; Eisenberg, E. Can free energy transduction be localized at some crucial part of the enzymatic cycle? *Q. Rev. Biophys.* **1981**, *14*, 463−511.
(27) Hill, T. L. Some general principles in free energy transduction. *Proc. Natl. Acad. Sci. U.S.A.* **1983**, *80*, 2922−2925.
(28) Raushel, F. M.; Thoden, J. B.; Holden, H. M. The amidotransferase family of enzymes: Molecular machines for the production and delivery of ammonia. *Biochemistry* **1999**, *38*, 7891−7899.
(29) Simon, M. I.; Strathmann, M. P.; Gautam, N. Diversity of G proteins in signal transduction. *Science* **1991**, *252*, 802−808.
(30) Wang, H.; Oster, G. The Stokes efficiency for molecular motors and its applications. *Europhys. Lett.* **2002**, *57*, 134.
(31) Qian, H. Motor protein with nonequilibrium potential: Its thermodynamics and efficiency. *Phys. Rev. E* **2004**, *69*, No. 012901.
(32) Thomas, W. E.; Vogel, V.; Sokurenko, E. Biophysics of catch bonds. *Annu. Rev. Biophys.* **2008**, *37*, 399−416.

DOI: 10.1021/acs.jpcb.7b10621
J. Phys. Chem. B 2018, 122, 1387−1393

(33) Brown, A. I.; Sivak, D. A. Allocating dissipation across a molecular machine cycle to maximize flux. *Proc. Natl. Acad. Sci. U.S.A.* **2017**, *114*, 11057−11062.
(34) Hill, T. *Free Energy Transduction in Biology: Steady State Kinetic and Thermodynamic Formalism*; Academic Press: New York, 1977.
(35) Hodges, A. R.; Krementsova, E. B.; Trybus, K. M. Engineering the processive run length of myosin V. *J. Biol. Chem.* **2007**, *282*, 27192−27197.
(36) Andreasson, J. O. L.; Milic, B.; Chen, G.-Y.; Guydosh, N. R.; Hancock, W. O.; Block, S. M. Examining kinesin processivity within a general gating framework. *eLife* **2015**, *4*, No. e07403.
(37) Muthukrishnan, G.; Zhang, Y.; Shastry, S.; Hancock, W. O. The processivity of kinesin-2 motors suggests diminished front-head gating. *Curr. Biol.* **2009**, *19*, 442−447.
(38) Nam, W.; Epureanu, B. I. Highly loaded behavior of kinesins increases the robustness of transport under high resisting loads. *PLoS Comput. Biol.* **2015**, *11*, No. e1003981.
(39) Topraka, E.; Yildiz, A.; Hoffman, M. T.; Rosenfeld, S. S.; Selvin, P. R. Why kinesin is so processive. *Proc. Natl. Acad. Sci. U.S.A.* **2009**, *106*, 12717−12722.
(40) Hinczewski, M.; Tehver, R.; Thirumalai, D. Design principles governing the motility of myosin V. *Proc. Natl. Acad. Sci. U.S.A.* **2013**, *110*, E4059−E4068.
(41) Zimmermann, E.; Seifert, U. Efficiencies of a molecular motor: A generic hybrid model applied to the F_1-ATPase. *New J. Phys.* **2012**, *14*, No. 103023.
(42) Fisher, M. E.; Kolomeisky, A. B. Simple mechanochemistry describes the dynamics of kinesin molecules. *Proc. Natl. Acad. Sci. U.S.A.* **2001**, *98*, 7748−7753.
(43) Hwang, W.; Hyeon, C. Quantifying the heat dissipation from a molecular motor's transport properties in nonequilibrium steady states. *J. Phys. Chem. Lett.* **2017**, *8*, 250−256.
(44) Liepelt, S.; Lipowsky, R. Kinesin's network of chemomechanical motor cycles. *Phys. Rev. Lett.* **2007**, *98*, No. 258102.
(45) Lau, A. W. C.; Lacoste, D.; Mallick, K. Nonequilibrium fluctuations and mechanochemical couplings of a molecular motor. *Phys. Rev. Lett.* **2007**, *99*, No. 158102.
(46) Singh, M. P.; Mallik, R.; Gross, S. P.; Yu, C. C. Modeling of single-molecule cytoplasmic dynein. *Proc. Natl. Acad. Sci. U.S.A.* **2005**, *102*, 12059−12064.
(47) Visscher, K.; Schnitzer, M. J.; Block, S. M. Single kinesin molecules studied with a molecular force clamp. *Nature* **1999**, *400*, 184−189.
(48) Carter, N. J.; Cross, R. A. Mechanics of the kinesin step. *Nature* **2005**, *435*, 308−312.
(49) Wang, Q.; Diehl, M. R.; Jana, B.; Cheung, M. S.; Kolomeisky, A. B.; Onuchic, J. N. Molecular origin of the weak susceptibility of kinesin velocity to loads and its relation to the collective behavior of kinesins. *Proc. Natl. Acad. Sci. U.S.A.* **2017**, *114*, E8611−E8617.
(50) Mukherjee, S.; Alhadeff, R.; Warshel, A. Simulating the dynamics of the mechanochemical cycle of myosin-V. *Proc. Natl. Acad. Sci. U.S.A.* **2017**, *114*, 2259−2264.
(51) Thorn, K. S.; Ubersax, J. A.; Vale, R. D. Engineering the processive run length of the kinesin motor. *J. Cell Biol.* **2000**, *151*, 1093−1100.
(52) Schnitzer, M. J.; Block, S. M. Kinesin hydrolyses one ATP per 8-nm step. *Nature* **1997**, *388*, 386−390.
(53) Hill, T. L. Interrelations between random walks on diagrams (graphs) with and without cycles. *Proc. Natl. Acad. Sci. U.S.A.* **1988**, *85*, 2879−2883.

DOI: 10.1021/acs.jpcb.7b10621
J. Phys. Chem. B 2018, 122, 1387−1393